# Complete Single Mode Condition for Silica-Titania Rib Waveguides on Glass Substrates

Cuma Tyszkiewicz, *Member, IEEE, Member, OSA*

***Abstract*—A single mode condition (SMC) for silica-titania rib waveguides on glass is the subject of this work. There are two mechanisms leading to the single mode propagation of a lightwave in rib waveguides. Considering waveguides whose rib width is greater than a thickness of a parent-slab waveguide, the one that would be created by extending the rib in the horizontal direction, the first mechanism is related to the leaking of $HE_{01}$ and $EH_{01}$ modes to slab waveguides on either side of the rib. The second mechanism is related to cut-off of those modes. Presented condition is expressed by two criterion functions. The first function, corresponding with the first mechanism, was introduced in our previous work describing the SMC for shallow rib waveguides. The second one, allowing to predict when the first order modes are cut-off is presented in this work. As a result, the complete SMC is formulated. It allows to predict a range of morphological parameters in which propagation is single mode, not only in shallow but also in deep rib waveguides. Moreover, considering the leaking of the $HE_{01}$ mode, it is shown that the prediction is accurate by using coefficients of criterion functions obtained by the linear interpolation.**

***Index Terms*—Integrated photonics, optical design, rib optical waveguides, single-mode conditions.**

## I. Introduction

RIB and strip waveguides are the core components in variety of optoelectronic [1],[2] and photonic devices [3],[4]. They are a part of many planar integrated circuit (PIC) designs. Single mode propagation is favorable, or even necessary, considering devices that are designed for application in integrated optic telecommunication systems, [5],[6] quantum communication applications [7] and integrated optic chemical and biochemical sensor systems [8]–[10], especially those which use the evanescent wave spectroscopy technique [11],[12]. Limiting our attention to devices belonging to the second group, it is interesting to note that rib waveguides are being used two different ways. They can be a part of an optical measurement transducer responsible for detection of a measurand directly [13],[14] or via interaction of the latter with a sensitive film [15],[16]. In this case PICs contain planar interferometers, which are converting variations in the optical phase to light intensity changes [17],[18]. Sensitivity of interferometric measurements is limited by interferometric contrast. Therefore application of single mode waveguides is necessary to achieve high interferometric contrast. As shown in the paper [19], the ability to guide the light in the single mode regime by SOI rib waveguides is necessary for resonant spectroscopy measurements. However, it is not the only reason to which single mode propagation regime is of the great importance. The homogeneous sensitivity of slab waveguides are maximum if those waveguides are single mode, have a step-index refractive index profile and their thickness is slightly greater than the cut-off thickness [20]. Whereas authors of the paper [9] showed that surface sensitivity of rib and strip waveguides is higher in a single mode propagation regime. The second function of rib and strip waveguides is the distribution of an optical wave among the components integrated in a PIC [21]–[23].

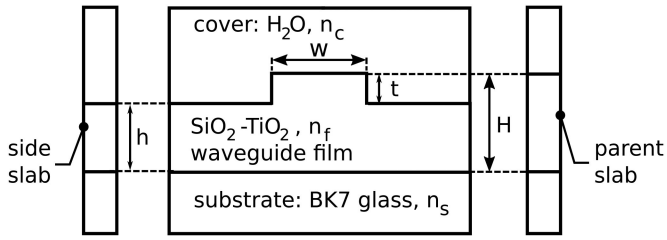


Fig. 1. Schematic of the rib waveguide investigated in this paper. A parent-slab is the slab waveguide having thickness $H$ whereas a side-slab is the slab waveguide having thickness $H$-$t$. Parameters description: $w$ - rib width, $t$ - rib height, $n_s$, $n_f$, $n_c$ - refractive indices of a substrate, waveguide film, and cover (ambient).

Research on single mode propagation conditions began with the search for such geometrical parameters of rib waveguides which allow to achieve efficient coupling between single mode rib waveguides and single mode optical fibers. Researchers began studying so called "large cross-section rib waveguides". As a result, several single mode conditions (SMC) for rib waveguides were formulated. They have a form of inequalities operating either directly on the morphological parameters of rib waveguides that are characterizing their transversal sizes - $H$, $w$ and $t$ (Fig. 1) - or on the dimensionless, effective parameters $u$ and $r$ derived using the equations in the footnote of (1). The first SMC was given by Petermann [24]. It was derived solely on a basis of the effective index method (EIM) [25],[26] and therefore is being referred as the EIM condition:

$$u < r/\left(1-r^2\right)^{1/2} \tag{1}$$

Manuscript received January 28, 2021; revised March 31, 2021; accepted April 14, 2021. Date of publication April 16, 2021; date of current version July 2, 2021. This work was supported by Polish National Science Center under Grant DEC-2017/25/B/ST7/02232.

The author is with the Department of Optoelectronics, Silesian University of Technology, 44-100 Gliwice, Poland (e-mail: cuma.tyszkiewicz@polsl.pl).

Color versions of one or more figures in this article are available at https://doi.org/10.1109/JLT.2021.3073805.

Digital Object Identifier 10.1109/JLT.2021.3073805

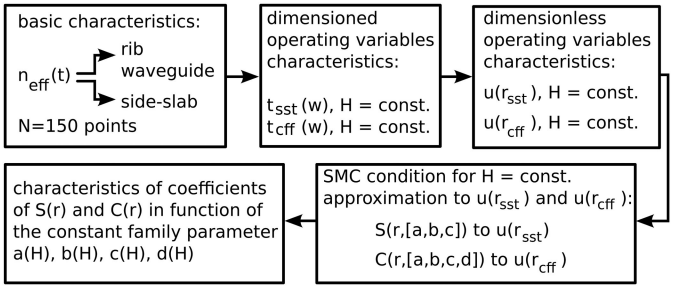


Fig. 2. The diagram presenting subsequent steps of the analysis presented in this paper. Morphological parameters of rib waveguides and side-slab waveguides are presented in Fig. 1. *S(r)*, *C(r)* - functions approximating $u(r_{sst})$ and $u(r_{cff})$, *a*,*b*,*c*,*d* - coefficients of *S*(*r*) and *C*(*r*).

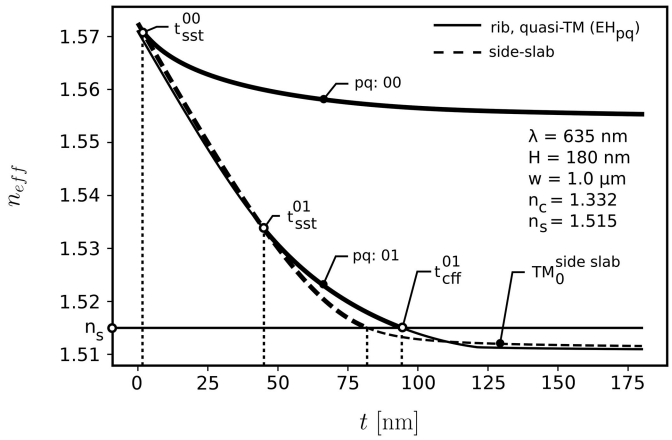


Fig. 3. Modal characteristics of rib waveguide *EH* modes and its associated side-slab waveguide $TM_0$ mode as a function of the rib height *t*.

where $u = w_{\text{eff}}/H_{\text{eff}}$, $r = h_{\text{eff}}/H_{\text{eff}}$, $h_{\text{eff}} = h+q$, $H_{\text{eff}} = H+q$, $w_{eff} = w+2\gamma_c/\{k(n_f^2-n_c^2)^{1/2}\}$, $q = \gamma_c/\{k(n_f^2-n_c^2)^{1/2}\}+\gamma_s/\{k(n_f^2-n_s^2)^{1/2}\}$, $n_f$, $n_s$ and $n_c$ are refractive indices of the guiding region, substrate and cover, respectively. The parameter $\gamma$ depends on a polarization of the guided wave, $\gamma_{c,s} = 1$ for $HE_{pq}$ modes (quasi-TE) and $\gamma_{c,s} = (n_{c,s}/n_f)^2$ for $EH_{pq}$ modes (quasi-TM). Finally, $k = 2\pi/\lambda$ where $\lambda$ is a wavelength. The equations in the footnote of (1) are from [27].

The EIM condition was reformulated by Soref *et al.* [28] by adding a constant parameter to its right-hand side. Moreover it is accompanied by a range of applicability provided by the second inequality:

$$u < a_S + r/\left(1-r^2\right)^{1/2} \tag{2}$$

$$0.5 \le r \le 1.0 \tag{3}$$

The authors reasoned that in this range the rib waveguide first order modes ($HE_{01}$ or $EH_{01}$) leak to slab waveguides on either side of the rib. The latter are further referred to as "side-slab" waveguides. In that range side-slab waveguides are thick enough to sustain the fundamental mode, of the corresponding polarization. Actually, the necessary condition, reflected by various SMC inequalities [28]–[34], is that effective indices of first order modes should be less than the effective index of the fundamental side-slab mode of the corresponding polarization. In majority of papers this inequality was derived for $HE_{01}$ and $EH_{01}$ modes. It has one of the following forms: $u<S(r)$ [24],[28],[30],[35], $u<S(r,H)$ [31]–[34] and $u<S(r,H,t,w)$ [29], where *S* is some continuous function. There are also papers dealing with rib waveguides in which $HE_{10}$ and $EH_{10}$ modes appear prior to $HE_{01}$ and $EH_{01}$ because $w<H$ [19].

There is also a second mechanism leading to the single mode propagation. Modal characteristics of rib waveguides are continuously decreasing functions of the rib height *t*, as one can observe in Fig. 3 placed in the section IIIA. If the parent slab thickness *H* is small enough, it is possible that a higher order mode is cut-off before a value of the rib height reaches $t = H$. A SMC inequality corresponding to this mechanism has a form of $u>C$, where *C* is also a continuous function of rib waveguides morphological parameters. So far the only SMC condition incorporating both mechanisms was presented in the paper [32]. Authors proposed the function of the same form for both *S* and *C*. However it has as many as seven free parameters and takes both *r* and *H* as its independent variables.

In this paper the SMC is formulated as a set of two inequalities: $u<S(r)$ and $u>C(r)$ corresponding to both described mechanisms. The new function *C*(*r*) is proposed. In association with the function *S*(*r*), presented in my former paper [35], they form a complete single mode propagation condition. Both of them have only one dimensionless independent variable *r*, which is an advantage over those SMC whose right-hand side is expressed also in terms of *H*, *t* or *w*.

So far investigations of single mode rib waveguides concerning directly SMCs [28],[29],[30],[32],[36],[37] or other properties of rib waveguides (e.g., birefringence) in a context of the SMC [31],[33],[38],[39], were carried predominantly for SOI waveguides. Nevertheless, there are also papers concerning rib waveguides characterized by refractive index values corresponding to other materials: GeSi-Si [28], polymer-silica [36], GaAs-AlGaAs [40], $Si_3N_4$-$SiO_2$ [41], Yb-YAG/YAG [34] and SiC-$SiO_2$ [42]. When it comes to rib geometry and calculation methods, researchers investigated vertical-walled [24],[27],[28],[36],[38],[32]–[34],[40],[43] and sloping-walled [29]–[31],[39] rib waveguides, using for this purpose the EIM [24],[28], the method of Film Mode Matching (FMM) [32]–[34],[36],[38],[44], the Beam Propagation Method (BPM) [29],[30],[37],[40],[45] and the Finite Element Method (FEM) [43],[46].

This paper presents the results of theoretical analysis of the SMC for silica-titania rib waveguides fabricated on glass substrates, using a sol-gel method [47]. These waveguides were elaborated with the intention of their application to design planar optical sensing transducers for chemical and biochemical sensors. Therefore, an assumed value of the ambient medium refractive index is equal to a value typical for water ($n_c = 1.332$ for $\lambda = 635$ nm). Analysis of the SMC for shallow rib waveguides in the aforementioned paper [35] was carried out for $n_c = 1.0$. The silica-titania rib waveguides investigated in this work have substantially higher aspect ratio ($w/H>8$),

than those investigated by the researchers cited in this paper ($w/H<4.5$). This way, results presented in this paper expand our knowledge about the single mode propagation conditions for rib waveguides.

## II. Method

Adopted methodology is shown in Fig. 2 in a form of the workflow diagram. The SMC was derived from the analysis of a rich set of effective index (modal) characteristics of rib waveguides and side-slab waveguides whose morphological parameters are described in Fig. 1. Modal characteristics were calculated as a function of the rib height $t$, using the rigorous and robust FMM method implemented in the FIMMWAVE 6.3 solver. As shown in the paper [37], the analysis relaying on modal characteristics is sufficient for rib waveguides that do not support higher order vertical modes, i.e., $HE_{pq}$ or $EH_{pq}$ modes having $p>1$. Silica-titania rib waveguides studied in this paper fulfill this condition. Directional couplers based on them are single mode despite the fact that effective indices of the first order horizontal modes $HE_{01}$ and $EH_{01}$ are bound – their effective indices are higher than the substrate refractive index [48].

Assuming that the thickness $H$ of the parent-slab waveguide is a constant parameter, one can associate a given modal characteristic $n_{eff}(t)$ of the side-slab waveguide with a set of rib waveguides modal characteristics, calculated for different value of the rib width $w$. The exemplary modal characteristics are presented in Fig. 3. One can observe from this figure, that there are two special values of the rib height. The first one, denoted by $t_{sst}$, is a value for which effective indices of rib waveguide modes are equal to an effective index of the fundamental mode of the associated side-slab waveguide. The second one, denoted by $t_{cff}$, is a value of the rib height for which the rib waveguide becomes cut-off: $n_{eff} = n_s$.

In the next step, obtained values of $t_{sst}$ and $t_{cff}$ were grouped into characteristics in function of width $w$ and transformed into a space of dimensionless variables ($r$,$u$) by using the equations written in the footnote of (1). As a result, two kinds of characteristics exist for the given value of $H$: $u(r_{sst})$ and $u(r_{cff})$. These characteristics were subsequently approximated. by the following functions:

$$u = S(r) = a + b \cdot r/\left(1 - r^2\right)^c \tag{4}$$

$$u = C(r) = a + b \cdot r/\left(c - r^2\right)^d \tag{5}$$

where $a$,$b$,$c$ and $d$ are approximation coefficients calculated by using the *curve_fit* method implemented in the Scientific Python environment [49]. As one can observe, $S(r)$ becomes identical to a function proposed by Soref (2) if $b = 1$ and $c = 0.5$. It is noteworthy that from a formal point of view $C(r)$ becomes $S(r)$ if $c = 1$ and $d$ becomes $c$. Finally the determined values of the approximation coefficients $a$,$b$,$c$ and $d$ were presented as the functions of the constant family parameter $H$.

Approximation errors were calculated for each approximated characteristic. A measure of the approximation error $E$ was defined as follows:

$$E = \frac{1}{N}\sum_{i=1}^{N}\frac{|u_i - u_{ai}|}{u_i} \tag{6}$$

where $u_i$ represents values of $u_{sst}$ and $u_{cff}$ characteristics, $u_{ai}$ represents values of approximating functions $S(r)$ and $C(r)$, $N$ is number of points on each characteristic. Both $u(r_{sst})$ and $u(r_{cff})$ are monotonic therefore each of them was determined in 60 points. The Soref's function (2) was also fitted to the $u(r_{sst})$ characteristics of $HE_{01}$ and $EH_{01}$ modes. The aim of this was to find if the function $S(r)$ gives better approximation. As a result, the values of the Soref's correction coefficient and of the approximation error were determined as functions of $H$.

Every $n_{eff}(t)$ characteristic was calculated in the interval $t \in < 0, H >$and has $N_0 = 150$ points. The values of the parent slab thickness $H$ varied from 135 nm to 240 nm with a step increase of 15 nm. The values of the rib width $w$ varied from 1.0 μm to 2.0 μm with a step increase of 0.02 μm. It was assumed that a wavelength is $\lambda = 635$ nm. The refractive indices of a waveguide film, glass substrate and ambient at this wavelength are $n_f = 1.8186$, $n_s = 1.5150$ and $n_c = 1.3320$, respectively.

## III. Results and Discussion

### A. Modal Characteristics

The exemplary modal characteristic of a silica-titania rib waveguide for *EH* modes and a side-slab waveguide are presented in Fig. 3. If a given mode of the rib waveguide or side-slab waveguide is guided, its characteristic is plotted using a solid, bold line. One can observe that the rib waveguide is single mode in two intervals of $t$: $(t^{00}_{sst}, t^{01}_{sst})$and $(t^{01}_{cff}, H)$. It is so because in the interval $(t^{01}_{sst}, t^{01}_{cff})$ the mode $EH_{01}$ is guided, whereas in the interval $(0, t^{00}_{sst})$both $EH_{00}$ and $EH_{01}$ leak into the side-slab. In the present context, the rib waveguide can be single modal in one or two intervals of $t$. depending on specific values of $H$, $w$, $n_c$ and on the polarization. This is because the parameters $t_{sst}$ and $t_{cff}$ does not always exist for polarization and mode orders relevant to the subject matter: $HE_{00}, EH_{00}, HE_{01}, EH_{01}$. The $t_{sst}$ for $HE_{00}$, in particular, does not exist in the considered range of morphological parameters.

### B. Characteristics of $T_{sst}$ and $T_{cff}$

Characteristics of $t_{sst}$ and $t_{cff}$ as a function of the rib width for a fixed value of the parent slab thickness have been obtained from modal characteristics. Staying with *EH* modes, such characteristics for the family of rib waveguides, whose parent slab thickness is $H = 180$ nm, are presented in Fig. 4. The mode $EH_{01}$ is not cut-off in all considered range of $w$. The value of $t_{cff}$ corresponding to it quickly reaches $H$ at some $w = w_t$, rendering the rib waveguide single modal in a single interval $(t^{00}_{sst}, t^{01}_{sst})$.

One can observe from Fig. 4 that calculation of the crucial values $t_{sst}$ and $t_{cff}$ is enough to determine whether the rib waveguide, having a certain value of the parent slab thickness $H$ and rib width $w$, is single mode or not. However, the main goal of this work is to formulate the SMCs using normalized rib width $u$ and normalized side-slab thickness $r$.

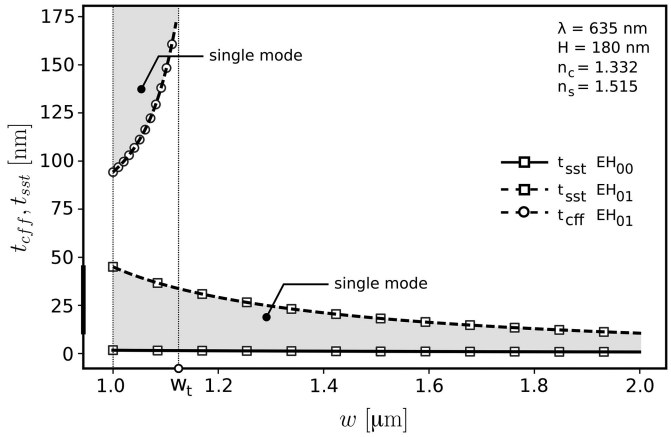


Fig. 4. Characteristics of the $t_{sst}$ and $t_{cff}$ as a functions of the rib width $w$.

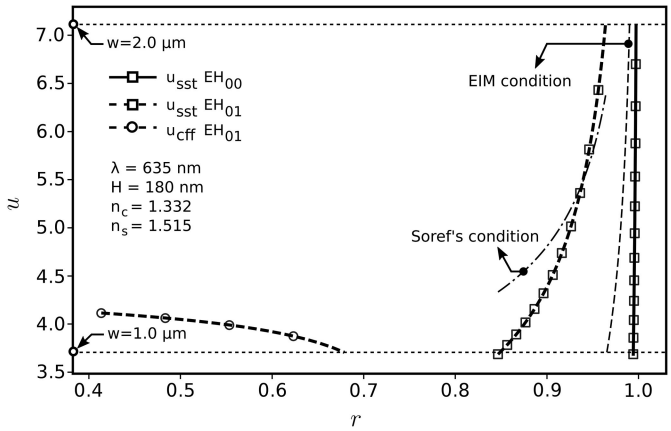


Fig. 5. Characteristics of the normalized rib width $u$ as a function of the normalized side-slab thickness $r$ corresponding to the $t_{sst}$ and $t_{cff}$ values of rib waveguides *EH* modes.

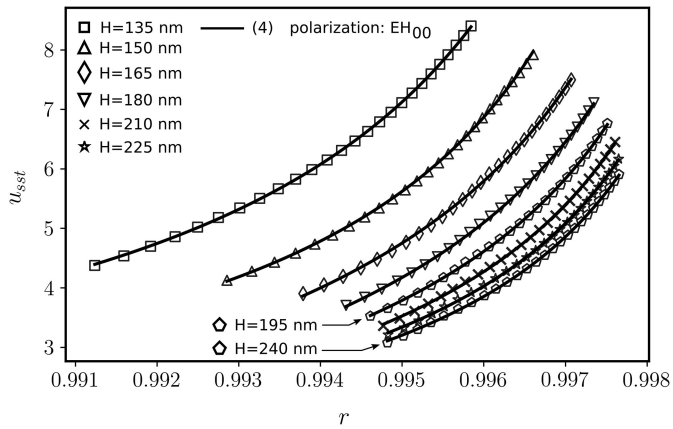


Fig. 6. Characteristics of the normalized rib width $u$ for which effective indices of $EH_{00}$ modes are equal to effective indices of the side-slab waveguide $TM_0$ mode. The solid lines are approximation curves calculated by using the function (4).

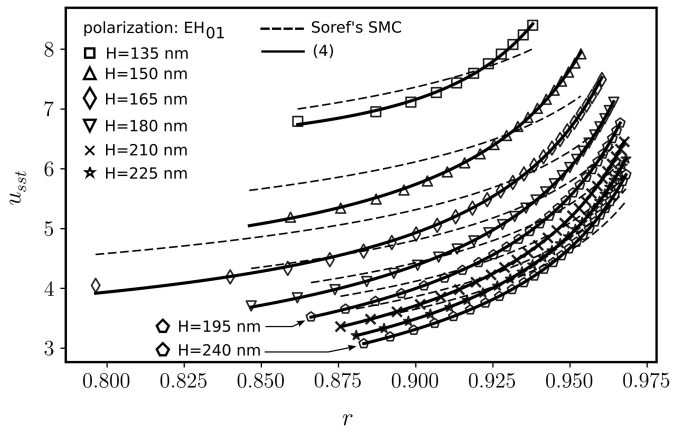


Fig. 7. Characteristics of the normalized rib width $u$ for which effective indices of $EH_{01}$ modes are equal to effective indices of the side-slab waveguide $TM_0$ mode. The dash and solid lines are approximation curves calculated by using the formulas (2) and (4), respectively.

### C. Single Mode Condition

The characteristics $t_{sst}(w)$ and $t_{cff}(w)$ of *EH* modes after conversion into normalized dimensionless parameters $u$ and $r$ are presented in Fig. 5. The values of $u_{sst}$ and $u_{cff}$, determined from modal characteristics, are marked with squares and circles, respectively. Every fifth marker was plotted in order to avoid obscuration of thick solid and dashed lines representing the values calculated using the functions $S(r)$ and $C(r)$ approximating $u_{sst}(r)$ and $u_{cff}(r)$, respectively. As one can see the functions (4) and (5), are an excellent approximation to the $u^{00}_{sst}$, $u^{01}_{sst}$ and $u^{01}_{cff}$characteristics. The dashed line representing the EIM condition (1) is a very poor approximation to the $u^{01}_{sst}$. This condition is better approximating the $u^{00}_{sst}$ characteristic. The Soref's condition (2) is the much better approximation to the $u^{01}_{sst}$ than the EIM condition. Calculated value of the Soref's correction coefficient is equal to $a_S = 2.74$. It is significantly different from the value 0.3 derived in Soref's work [28]. That is because rib waveguides considered in this work have an aspect ratio in a different range. It was shown in [35] and also in this work is confirmed by characteristics showing how $a_s$ is varying with the rib height $H$.

The range of $u$ values returned by the Soref's condition is not extended to an overall range determined by the minimum and maximum value of $w$. This is due to the fact that the values of $r$ introduced into (2) were not calculated for the interval (0,$H$), but for the range of $t_{cff}$ values of the $EH_{01}$ mode. It is indicated by a bold line on the vertical axis in Fig. 4. A different procedure was applied in the case of the EIM condition. The $r$ values were calculated for an overall range of $u$ by using (2) inverted. Otherwise, calculating $u$ for the same interval of $r$ as in the case of the Soref's condition, one would get as a result a characteristic lying below the horizontal line corresponding to $w = 1.0$ μm (Fig. 5).

The characteristics $u^{00}_{sst}$ , $u^{01}_{sst}$ and $u^{01}_{cff}$were determined for more than one value of the parent-slab thickness $H$ in order to check whether the functions (4) and (5) give equally well approximation in a broad range of $u$ values. In Figs 6, 7, 8, and 9 are presented series of $u^{00}_{sst}$, $u^{01}_{sst}$ and $u^{01}_{cff}$ characteristics and functions approximating them. Only $u^{01}_{sst}$ characteristics are presented for both polarizations (Figs. 7 and 8). Considering the

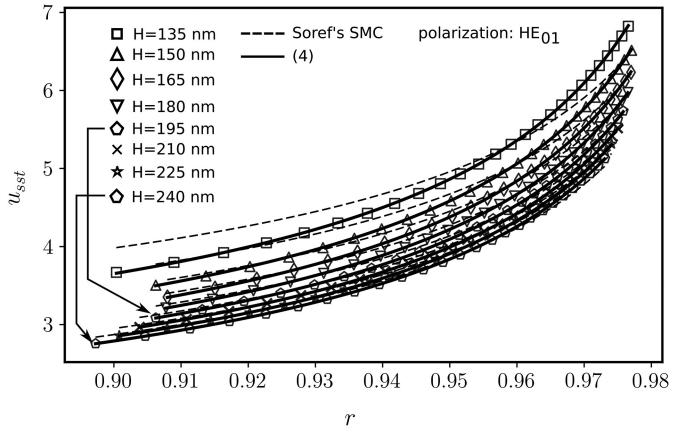


Fig. 8. Characteristics of the normalized rib width *u* for which effective indices of $HE_{01}$ modes are equal to effective indices of the the side-slab waveguide $TE_0$ mode. The dash and solid lines are approximation curves calculated by using the the Soref's function (2) and function (4), respectively.

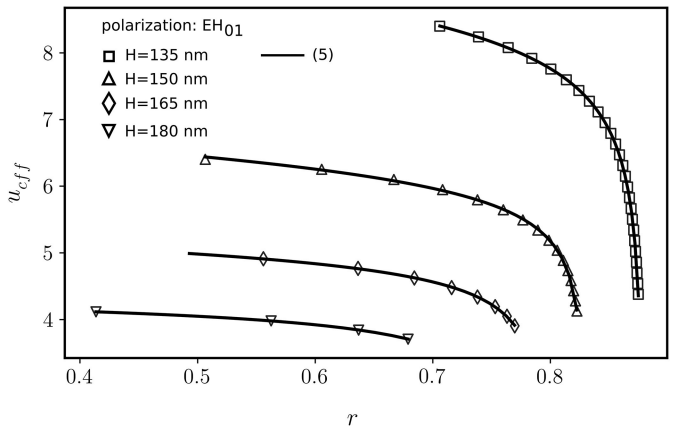


Fig. 9. Characteristics of the normalized rib width *u* for which $EH_{01}$ modes are cut-off. The solid lines are approximation curves calculated by using the function (5).

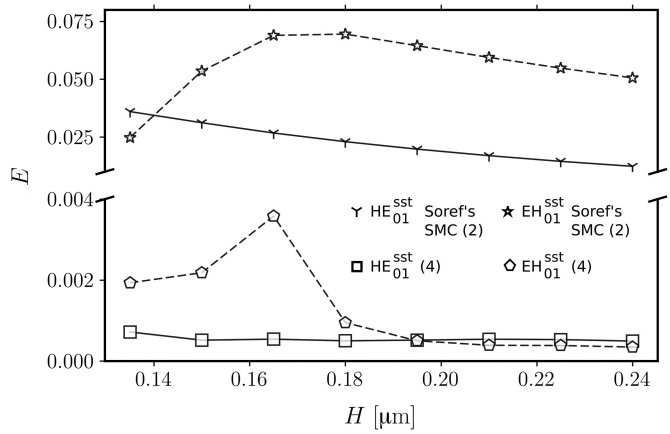


Fig. 10. Values of the approximation error *E* for $u_{sst}$ characteristics of $HE_{01}$ and $EH_{01}$ modes, approximated by using the Soref's function (2) and function (4).

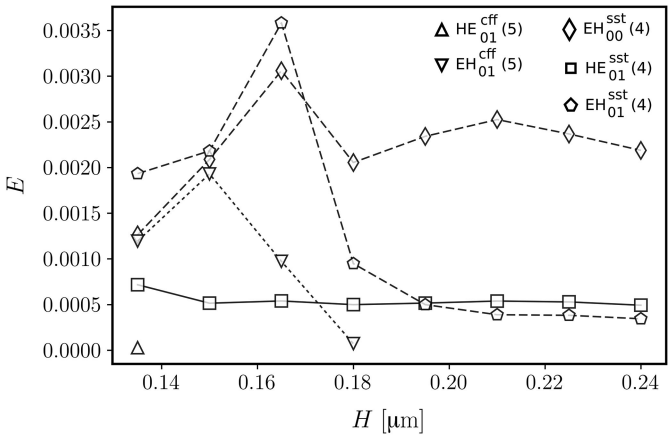


Fig. 11. Values of the approximation error *E* for $u_{sst}$ and $u_{cff}$ characteristics approximated by using the functions (4) and (5), respectively.

$EH_{01}$ mode, there are no characteristics of $u_{cff}^{01}$ for $H \geq 195$ nm because this mode is not cut-off. The same situation take place for $HE_{01}$ modes but this time for $H \geq 150$ nm. There are no $u_{sst}^{00}$ characteristics for $HE_{00}$ modes in the considered range of *H*. It is worth noticing that (5) gives very good approximation to $u_{cff}^{01}$ (Fig. 9) even though the first derivative of $u_{cff}^{01}$ varies significantly with increasing values of the parent slab thickness *H*. The intervals of *r*-values in which $HE_{01}$ and $EH_{01}$ modes are leaky, belong to the interval (3).

Values of the approximation error, *E*, were calculated by using (6). They are presented as a functions of the parent slab thickness, *H*, in Figs 10 and 11 . The lines on these figures are only for guiding the eyes. Approximation error values of $u_{sst}^{01}$ modes are presented in Fig. 10. One can observe that in considered range of *H*, the approximation error for the Soref's function (2) is several times higher than for (4). Considering approximation of $u_{sst}$ characteristics for $EH_{01}$ modes by using (4), one can see a local maximum of the approximation error for $H = 165$ nm. It results from weaker fit at the beginning of the corresponding fit interval (see Fig. 7). In this respect it is to be noted that its magnitude is the greatest for all considered $u_{sst}^{01}$ characteristics. Moreover, one can see similar behavior of characteristics approximated by (2) and (4), namely for $H < 165$ nm the approximation error is decreasing for decreasing values of *H*. This may be explained by the fact that $EH_{01}$ modes become weakly guided for $H < 165$ nm. Nevertheless, approximation of $u_{sst}^{01}$ characteristics with (4) gives small errors, which confirms that this function is a good approximation to $u_{sst}$ for both $HE_{01}$ and $EH_{01}$ modes.

The plots presented in Fig. 11 prove that (4) is also very good approximation to $u_{sst}$ characteristics of $EH_{00}$ modes. However, a magnitude of the approximation error for this mode order is greater than for $EH_{01}$ modes. Most of all, one can observe from Fig. 11 that the newly proposed function $C(r)$ gives very good approximation to $u_{cff}$ characteristics.

A flow chart diagram of the algorithm allowing to determine whether a given rib waveguide is single mode is presented in the Appendix.

Finally, the relationship between the Soref's coefficient $a_s$ and the parent slab waveguide thickness *H* indicates that the

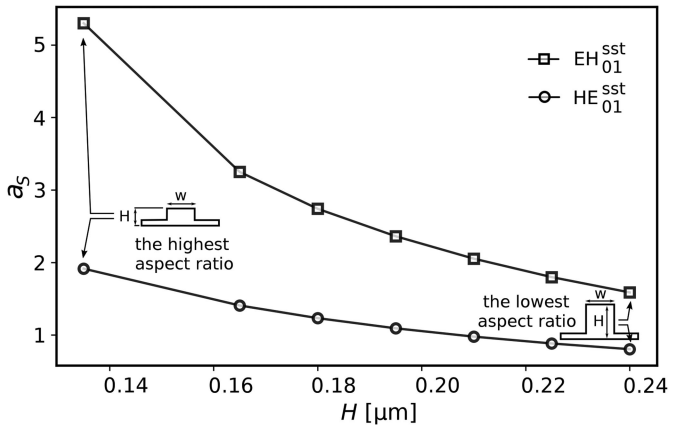


Fig. 12. Values of the Soref's correction coefficient with respect to the parent slab thickness $H$ for polarizations *HE* and *EH*.

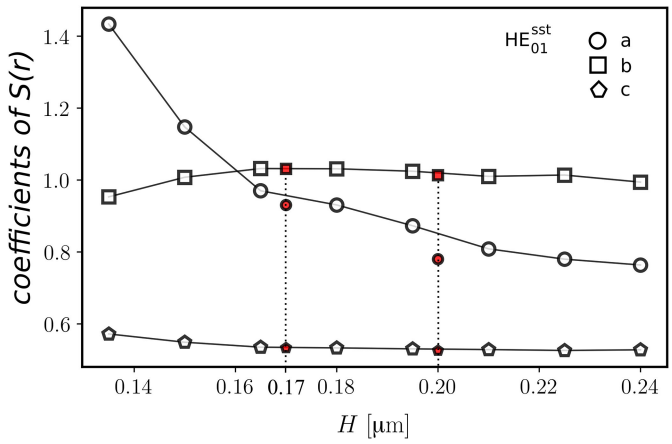


Fig. 13. Coefficients of the $S(r)$ criterion function with respect to the parent slab thickness $H$ for the quasi $TE_{01}$ mode. Coefficients for $H = 0.17$ and 0.20 μm were obtained by the linear interpolation.

magnitude of that coefficient depends predominantly on the rib waveguide aspect ratio. They behave similarly as the ones for the cover refractive index $n_c = 1.0$ which are presented in [35] on Fig. 8b.

### *D. Single Mode Condition Based on Interpolated Criterion Functions Coefficients*

So far it has been shown that in order to determine the coefficients $a$, $b$, $c$ and $d$ of the criterion functions, $S(r)$ and $C(r)$, it is necessary to select a value of the parent slab thickness $H$, determine a set of modal characteristics in a desired range of the rib width and carry out the approximation process. Suppose that we have two sets of those coefficients, for two different values ($H_1$ and $H_2$) and that there is a value $H_3 \in (H_1, H_2)$ for which those coefficients are unknown. One can put a question if the prediction about a value of the rib height for which a waveguide becomes multimode will be correct provided that the unknown coefficients $a$, $b$, $c$ and $d$ will be linearly interpolated. In order to answer to the problem put this way, the criterion functions coefficients were determined two ways for the two additional values of $H$: 0.17 μm and 0.20 μm. The values obtained by the procedure outlined in Fig. 2 are indicated by shaded markers in Figs. 13 -16. These graphs show criterion functions coefficients with respect to the parent slab thickness $H$. The linearly interpolated coefficients are on the intersection of the lines linking the white-faced markers and vertical dotted lines.

Considering the $HE_{00}$ mode, there are no characteristics of the $S(r)$ and $C(r)$ functions. That is because in the considered range of $H$ there are no $t_{sst}^{00}$ values, whereas $t_{cff}^{01}$ exists only for $H = 135$ nm. One can observe from the plots in Figs. 13-16 that linearly interpolated coefficients are greater or less to some extent than those obtained by the procedure outlined in Fig. 2. The particularly big difference exists for the coefficient a of the $S(r)$ of the $EH_{00}$ mode. The more comprehensive picture is unfolded on a characteristic of the approximation error (6), which is shown in Fig. 17. Error values for the criterion functions calculated using the linearly interpolated coefficients are indicated by shaded markers.

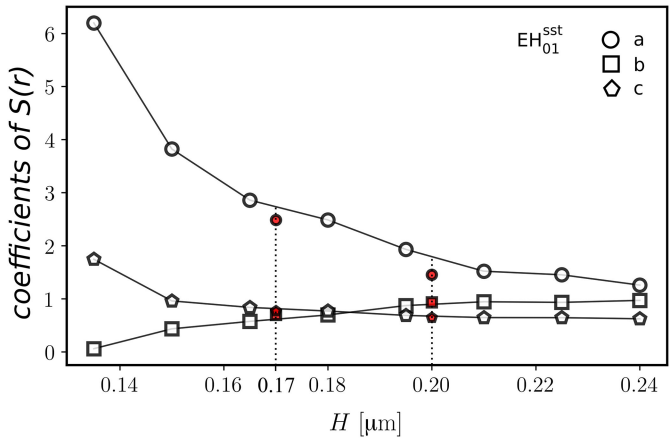


Fig. 14. Coefficients of the $S(r)$ criterion function with respect to the parent slab thickness $H$ for the quasi $TM_{01}$ mode. Coefficients for $H = 0.17$ and 0.20 μm were obtained by the linear interpolation.

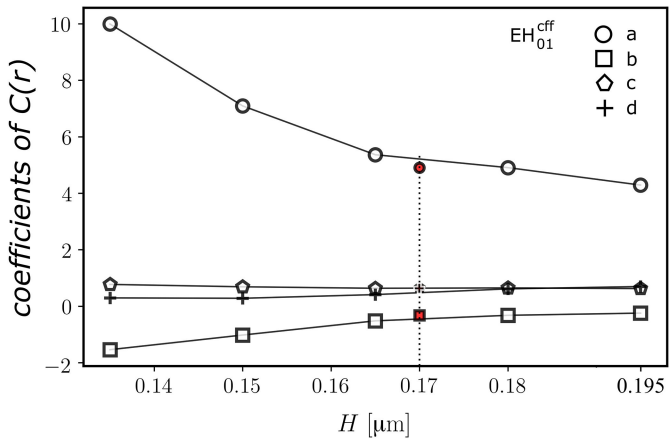


Fig. 15. Coefficients of the $C(r)$ criterion function with respect to the parent slab thickness $H$ for the quasi $TM_{01}$ mode. Coefficients for $H = 0.17$ and 0.20 μm were obtained by the linear interpolation.

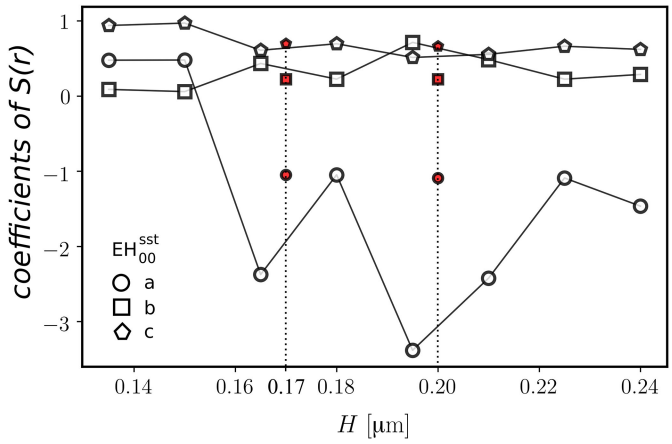


Fig. 16. Coefficients of the $S(r)$ criterion function with respect to the parent slab thickness $H$ for the quasi $TM_{00}$ mode. Coefficients for $H = 0.17$ and 0.20 μm are indicated by shaded markers.

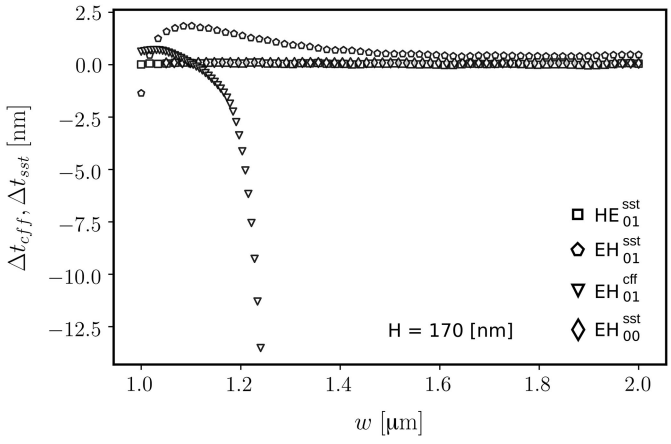


Fig. 18. The difference between values of $t_{sst}$ and $t_{cff}$ determined in the first case from criterion functions $S(r)$ and $C(r)$ and from modal characteristics $n_{eff}(t)$ in the second case. A thickness of the parent slab is $H = 170$ [nm].

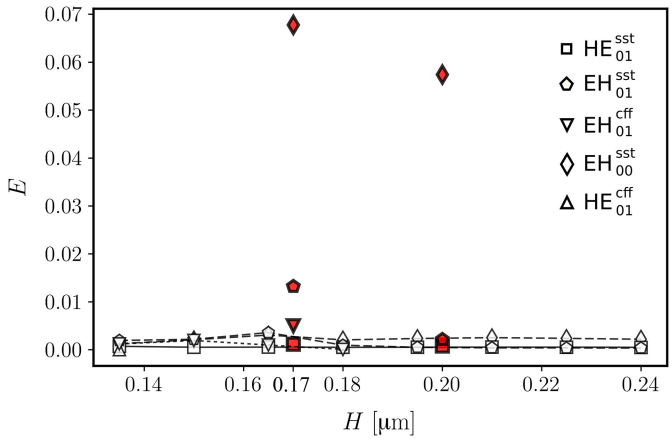


Fig. 17. Values of the approximation error for $u_{sst}$ and $u_{cff}$ characteristics. Those for $H = 0.17$ and 0.20 μm were calculated using criterion function whose coefficients were determined by the linear interpolation.

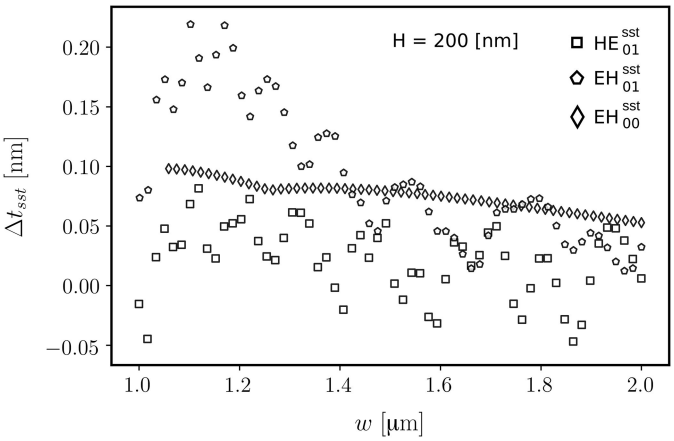


Fig. 19. The difference between values of $t_{sst}$ determined in the first case from the criterion function $S(r)$ and from modal characteristics $n_{eff}(t)$ in the second case. A thickness of the parent slab is $H = 200$ [nm].

The approximation error $E$ made with the $S(r)$ function whose coefficients were obtained by the linear interpolation is the lowest for the $HE_{01}$ mode and the greatest for the $HE_{00}$ mode. In the latter case it may be caused by relatively narrow interval from which $r$ takes its values. As regards the $C(r)$ function, taking into account adopted gradation of the parent slab thickness, the $t_{cff}(w)$ or $u_{cff}(r)$ characteristics exist only for the $EH_{01}$ mode and for $H<195$ nm. One can see that the approximation error for $H = 170$ nm is approximately 10 times greater than the value predicted from the corresponding characteristic in Fig. 11.

Finally, in order to assess a relation between a magnitude of the approximation error $E$ and the conformation to single mode propagation regime, the last type of characteristic is presented in Fig. 18 and 19. They are showing the difference between values of $t_{sst}$ and $t_{cff}$ determined from criterion functions, whose coefficients are linearly interpolated, and those obtained from the initial set of modal characteristics. An example of the latter is shown in Fig. 4.

One can observe from characteristics presented above, that values of $t_{sst}$ are approximated significantly better than values of $t_{cff}$. The absolute of $\Delta t_{cff}$ is increasing sharply, finally exceeding 12 nm. This stems from the fact that the function $C(r)$ has greater number of parameters than $S(r)$. The smallest differences are observed for $t_{sst}$ of the $HE_{01}$ mode. They do not exceed 0.1 nm, which is less than the accuracy of AFM measurements in vertical direction [50]. Interestingly, values of $\Delta t_{sst}$ of the $EH_{00}$ does not exceed 0.2 nm, for both $H = 170$ and 200 nm, even though a magnitude of the approximation error for this mode is the greatest. But as one can see in Figs. 17 and 18, taking into account the $EH_{01}$ mode, even though the error for $\Delta t_{sst}$ is smaller ($\sim$0.014), the magnitude of $\Delta t_{sst}$ exceeds 1 nm in broad range of values of the rib width $w$.

The analysis carried out in this section is showing that criterion functions whose parameters are linearly interpolated

cannot provide satisfactory approximation to $t_{sst}$ and $t_{cff}$ for both polarizations and all modes involved in the complete single mode condition. One can observe the oscillatory behavior in Fig. 16. Namely, the decrease in values of the coefficient $a$ (circle marker) is accompanied by increase in values of the coefficient $b$ (square marker), $H = 0.165$, 0.18 and 0.195 μm. If variations of these coefficients with respect to the parents slab thickness $H$ were monotonous then one would expect that the linear interpolation would give smaller errors for decreasing distance between the interpolation nodes $H_i$. The transformation of the original geometric parameters of rib waveguides ($H$, $w$ and $t$) to dimensionless parameters ($u$,$r$) may be the source of such behavior. As result of it the dimensionless side-slab thickness $r$ is limited to some subinterval of the interval $r \in (0, 1)$making approximation more difficult. Probably approximation of $t_{sst}(w)$ and $t_{cff}(w)$ would give better results.

## IV. Conclusion

The single mode condition presented in this work is composed of two criterion functions. It allows to resolve whether a rib waveguide conforms to single mode propagation regime, both as the result of leaking of first order modes into adjacent slab waveguides, or as the result of first order modes being cut-off. Both criterion functions in broad range of parent slab thickness values give very good approximation to normalized $u(r)$ characteristics corresponding with two mechanisms leading to single mode propagation. Coefficients of the criterion functions are only varying with the parent slab thickness. Therefore, one can try to calculate their values using linear interpolation in a range determined by two values of the parent slab thickness for which those coefficients are determined by fitting the criterion functions. As shown in the section III.D, only the rib height for which $HE_{01}$ modes start leaking into adjacent slabs, are well approximated by the criterion function $S(r)$ whose coefficients have been obtained by linear interpolation.

It must be made clear that in order to determine the coefficients $a$, $b$, $c$ and $d$ of the criterion functions $S(r)$ and $C(r)$, it is necessary to generate characteristics $t_{sst}(w)$ and $t_{cff}(w)$ whose knowledge is sufficient to determine single mode propagation range. As practical matter, calculation of $t_{sst}$ and $t_{cff}$ is more than enough if one searches for a single mode propagation range in some space of rib waveguides having the same parent slab thickness. Transformation to rib waveguide dimensionless and effective geometric parameters ($r$,$u$) is necessary if one wants to establish the criterion functions and compare them with others presented in the literature. The method proposed in this work may find practical application. Namely as an element of an optical CAD software that perform optimization of more complex structures (e.g., directional couplers, ring resonators) embodying rib waveguides that should operate in single mode propagation regime. However, the necessary condition is the possibility to operate on interpolated coefficients of the criterion functions. In that case it would not need to be necessary to calculate $t_{sst}$ and $t_{cff}$ for any change of the parent slab thickness $H$ and rib width $w$.

## Appendix

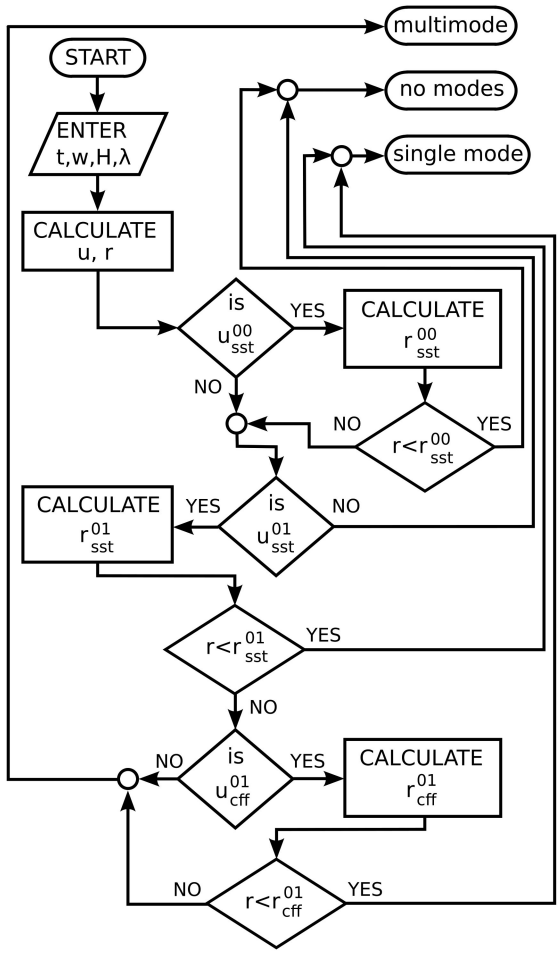


Fig. 20. A flow chart diagram of the algorithm for determination whether a rib waveguide is single mode. Values of functions $u_{sst}$ and $u_{cff}$ are calculated based on adequate coefficients $a$, $b$, $c$ and $d$.

## References


[1] J. Tang *et al.*, "Integrated optoelectronic oscillator," *Opt. Exp.*, vol. 26, no. 9, 2018, doi: 10.1364/OE.26.012257.

[2] Z. Zhu *et al.*, "Highly sensitive, broadband microwave frequency identification using a chip-based Brillouin optoelectronic oscillator," *Opt. Exp.*, vol. 27, no. 9, 2019, doi: 10.1364/OE.27.012855.

[3] S. Swagata, D. K. Pradip, B. Pallab, and G. Pranabendu, "A 1×2 polarization-independent power splitter using three-coupled silicon rib waveguides," *J. Opt.,* vol. 20, 2018, Art. no. 095801, doi: 10.1088/2040-8986/aad449.

[4] B. Y. Yu and X. Zhang, "Multimode waveguide crossing with ultralow loss and low imbalance," *Opt. Exp.*, vol. 28, no. 10, pp. 14705–14711, 2020, doi: 10.1364/OE.392445.

[5] M. F. Rosa *et al.*, "Design of a carrier-depletion Mach-Zehnder modulator in 250nm silicon-on-insulator technology," *Adv. Radio Sci.*, vol. 15, pp. 269–281, 2017, doi: 10.5194/ars-15-269-2017.

[6] C. Errando-Herranz, S. Das, and K. B. Gylfason, "Suspended polarization beam splitter on silicon-on-insulator," *Opt. Exp.*, vol. 23, no. 3, 2018, doi: 10.1364/OE.26.002675.

[7] R. Yusof, N. Ali, P. Kolenderski, K. Slowik, and N. A. M. A. Hambali, "Comparative studies of rib waveguide material for quantum communication application," *IOP Conf. Ser. Mater. Sci. Eng.*, vol. 551, 2019, Art. no. 012018, doi: 10.1088/1757-899X/551/1/012018.

[8] D. M. Kita, J. Michon, S. G. Johnson, and J. Hu, "Are slot and subwavelength grating waveguides better than strip waveguides for sensing?," *Optica*, vol. 5, no. 9, pp. 1046–1054, 2018, doi: 10.1364/OPTICA.5.001046.

[9] T. H. Talukdar, G. D. Allen, I. Kravchenko, and J. D. Ryckman "Single-mode porous silicon waveguide interferometers with unity confinement factors for ultra-sensitive surface adlayer sensing," *Opt. Exp.*, vol. 27, no. 16, 2019, doi: 10.1364/OE.27.022485.

[10] C. A. Barrios, "An analysis of a compact label-free guiding-wave biosensor based on a semiconductor-clad dielectric strip waveguide," *Sensors*, vol. 20, no. 12, 2020, Art. no. 3368, doi: 10.3390/s20123368.

[11] J. E. Midwinter, " On the use optical waveguide techniques for internal reflection spectroscopy," *IEEE J. Quantum Electron.*, vol. 7, no. 7, pp. 339–344, Jul. 1971, doi: 10.1109/JQE.1971.1076805.

[12] W. Lukosz, "Integrated optical chemical and direct biochemical sensors," *Sens. Actuator B Chem.*, vol. 29, no. 1-3 pp. 37–50, 1995, doi: 10.1016/0925-4005(95)01661-9.

[13] B. Kumari, R. K. Varshney, and B. P. Pal, "Design of chip scale silicon rib slot waveguide for sub-ppm detection of $N_2O$ gas at mid-IR band," *Sens. Actuator B Chem.*, vol. 255, pp. 3409–3416, 2018, doi: 10.1016/j.snb.2017.09.170.

[14] C. Ranacher *et al.*, "Mid-infrared absorption gas sensing using a silicon strip waveguide," *Sens. Actuator A Phys.*, vol. 277, pp. 117–123, 2018, doi: 10.1016/j.sna.2018.05.013.

[15] A. K. Pal, N. J. Goddard, H. J. Dixon, and R. Gupta, "A self-referenced diffraction-based optical leaky waveguide biosensor using photofunctionalised hydrogels," *Biosensors*, vol. 10, no. 10, 2020, Art. no. 134, doi: 10.3390/bios10100134.

[16] M. Angelopoulou *et al.*, "Rapid detection of mozzarella and feta cheese adulteration with cow milk through a silicon photonic immunosensor," *Analyst*, vol. 146, pp. 529–537, 2021, doi: 10.1039/d0an01706j.

[17] H. Saghaei, P. Elyasi, and R. Karimzadeh, "Design, fabrication, and characterization of Mach–Zehnder interferometers," *Photon. Nanostruct.*, vol. 37, 2019, Art. no. 100733, doi: 10.1016/j.photonics.2019.100733.

[18] Y. Xie, M. Zhang, and D. Dai, "Design rule of Mach-Zehnder interferometer sensors for ultra-high sensitivity," *Sensors*, vol. 20, p. 2640, 2020, doi: 10.3390/s20092640.

[19] A. Leblanc-Hotte, J. S. Delisle, S. Lesage, and Y. A. Pete, "The importance of single-mode behavior in silicon-on-insulator rib waveguides with very large cross section for resonant sensing applications," *IEEE J. Sel. Top. Quantum Electron.*, vol. 22, no. 6, pp. 241–248, 2016, doi: 10.1109/jstqe.2016.2545634.

[20] P. Karasiński, "Influence of waveguide parameters on the difference interference in optical planar structure," *Optica Applicata*, vol. 32, no. 4, pp. 775–796, 2002.

[21] N. Zamhari and A. A. Ehsan, "Large cross-section rib silicon-on-insulator (SOI) S-bend waveguide," *Optik*, vol. 130, pp. 1414–1420, 2017, doi: 10.1016/j.ijleo.2016.11.161.

[22] J. X. B. Sia *et al.*, "Mid-Infrared, ultra-broadband, low-loss, compact arbitrary power splitter based on adiabatic mode evolution," *IEEE Photon. J.,* vol. 11, no. 2, pp. 1–11, Apr. 2019, doi: 10.1109/JPHOT.2019.2907788.

[23] Q. Xu *et al.*, "An ultra-broadband polarizing beam splitter/coupler using asymmetric-waveguides," *Opt. Commun.*, vol. 454, 2020, Art. no. 124424, doi: 10.1016/j.optcom.2019.124424.

[24] K. Petermann, "Properties of optical rib-guides with large cross-section," *Archiv fur Electronik und Ubertragungstechnik (Germany)*, vol. 30, pp. 139–140, 1976.

[25] G. B. Hocker and W. K. Burns, "Mode dispersion in diffused channel waveguides by the effective index method," *Appl. Opt.*, vol. 16, pp. 113–118, 1977.

[26] K. S. Chiang, "Analysis of optical fibers by the effective-index method," *Appl. Opt.*, vol. 25, no. 3, pp. 348–354, 1986.

[27] S. P. Pogossian, L. Vescan, and A. Vonsovici, "The single-mode condition for semiconductor rib waveguides with large cross section," *J. Lightw. Technol.*, vol. 16, no. 10, pp. 1851–1853, 1998, doi: 10.1109/50.721072.

[28] R. A. Soref, J. Schmidtchen, and K. Petermann, "Large single-mode rib waveguides in gesi-Si and Si-on-si$O_2$," *IEEE J. Quantum Electron.*, vol. 27, no. 8, pp. 1971–1974, Aug. 1991.

[29] O. Powell, "Single-mode condition for silicon rib waveguides," *J. Lightw. Technol.*, vol. 20, no. 10, pp. 1851–1855, 2002, doi: 10.1109/JLT.2002.804036.

[30] X. Jinsong and Y. Jinzhong, "Single-mode condition for silicon rib waveguides with trapezoidal cross-section," *Opt. Commun.*, vol. 230, no. 4-6, pp. 253–257, 2004, doi: 10.1016/j.optcom.2003.11.031.

[31] S. P. Chan *et al.*, "Single-mode and polarization-independent silicon-on-insulator waveguides with small cross section," *J. Lightw. Technol.*, vol. 23, no. 6, pp. 2103–2111, 2005, doi: 10.1109/jlt.2005.849883.

[32] X. Xu, S. Chen, J. Yu, and X. Tu, "An investigation of the mode characteristics of SOI submicron rib waveguides using the film mode matching method," *J. Opt. A-Pure Appl. Opt.*, vol. 11, 2009, Art. no. 015508, doi: 10.1088/1464-4258/11/1/015508.

[33] B. A. Dorin and W. N. Ye, "Conditions for single-mode and birefringence-free ultrasmall SOI rib waveguides at 1310 nm," *J. Lightw. Technol.*, vol. 31, no. 21, pp. 3420–3424, 2013, doi: 10.1109/jlt.2013.2283374.

[34] M. Ziyang *et al.*, "Theoretical study of weakly-guided large-mode-area rib waveguides: Single-mode condition, birefringence, and super-mode generation," *Opt. Quantum Electron.,* vol. 48, 2016, Art. no. 554, doi: 10.1007/s11082-016-0828-z.

[35] C. Tyszkiewicz, "Single mode condition for shallow silica–titania rib waveguides," *Opt. Quantum Electron.*, vol. 50, 2018, Art. no. 360, doi: 10.1007/s11082-018-1627-5.

[36] R. Hauffe, U. Siebel, K. Petermann, and C. Kostrzewa, "The single mode condition for rib waveguides, revised," in *Proc. OSA/IPR*, 1999, pp. 112–114, doi: 10.1364/IPR.1999.RMH8.

[37] J. Lousteau *et al.*, "The single-mode condition for silicon-on-insulator optical rib waveguides with large cross section," *J. Lightw. Technol.*, vol. 22, no. 8, pp. 1923–1929, 2004, doi: 10.1109/JLT.2004.832427.

[38] L. Vivien *et al.*, "Polarization-independent single-mode rib waveguides on silicon-on-insulator for telecommunication wavelengths," *Opt. Commun.*, vol. 210, no. 1/2, pp. 43–49, 2002, doi: 10.1016/S0030-4018(02)01681-4.

[39] M. M. Milosevic and P. S. Matavulj, "Design rules for single-mode and polarization-independent silicon-on-insulator rib waveguides using stress engineering," *J. Lightw. Technol.*, vol. 23, no. 13, pp. 1840–1846, 2008, doi: 10.1109/jlt.2008.922193.

[40] A. D. Ferguson *et al.*, "Low-loss, single-mode GaAs/AlGaAs waveguides with large core thickness," *IEE Proc.-Optoelectron.*, vol. 156, no. 2, pp. 51–56, 2006, doi: 10.1049/ip-opt:20050024.

[41] R. R. Grote and L. C. Bassett, "Single-mode optical waveguides on native high-refractive-index substrates," *APL Photon.*, vol. 1, no. 7, 2016, doi: 10.1063/1.4955065.

[42] W. Du, Z. Chen, and F. Zhao, "Analysis of single-mode optical rib waveguide in silicon carbide," *Microw. Opt. Technol. Lett.*, vol. 55, no. 11, pp. 2636–2640, 2013, doi: 10.1002/mop.

[43] H. Huang, K. Liu, B. Qi, and V. J. Sorger, "Re-Analysis of single-mode conditions for silicon rib waveguides at 1550 nm wavelength," *J. Lightw. Technol.*, vol. 34, no. 16, pp. 3811–3817, 2016, doi: 10.1109/jlt.2016.2579163.

[44] A. S. Sudbo, "Film mode matching: A versatile numerical method for vector mode field calculations in dielectric waveguides," *Pure Appl. Opt.*, vol. 2, no. 3, pp. 211–233, 1993.

[45] J. V. Roey, J. V. D. Donk, and P. E. Lagasse, "Beam-propagation method: Analysis and assessment," *J. Opt. Soc. Amer.*,vol. 71, no. 7, pp. 803–810, 1981.

[46] M. Laurentis, A. Irace, and G. Breglio, "Determination of single mode condition in dielectric rib waveguide with large cross section by finite element analysis," *J. Comput. Electron.*, vol. 6, pp. 285–287, 2007, doi: 10.1007/s10825-006-0124-4.

[47] P. Karasiński and R. Rogoziński, "Rib waveguides fabricated by means of chemical etching of sol-gel films si$O_2$:Ti$O_2$," *Opt. Commun.*, vol. 245, no. 1-6, pp. 237–242, 2005, doi: 10.1016/j.optcom.2004.10.074.

[48] C. Tyszkiewicz, P. Karasiński, and R. Rogoziński, "Directional couplers fabricated via a sol–gel route and conventional optical lithography," *Opt. Quantum Electron.*, vol. 49, 2016, Art. no. 19, doi:10.1007/s11082-015-0283-2.

[49] P. Virtanen *et al.*, "SciPy 1.0: Fundamental algorithms for scientific computing in python," *Nat. Methods*, vol. 17, pp. 261–272, 2020, doi: 10.1038/s41592-019-0686-2.

[50] G. Dai *et al.*, "Development of a 3D-AFM for true 3D measurements of nanostructures," *Meas. Sci. Technol.*, vol. 22, Art. no. 094009, 2011, doi: 10.1088/0957-0233/22/9/094009.


**Cuma Tyszkiewicz** (Member, IEEE) received the M.S. and Ph.D. degrees in physics from the Faculty of Mathematics and Physics, Silesian University of Technology, Gliwice, Poland, in 2001 and 2006, respectively. After spending three years with the Institute of Physics, he joined the Department of Optoelectronics, Faculty of Electrical Engineering, as an Assistant Professor. In 2019, he was promoted to an Associate Professor of electrical engineering. His current research interests include theoretical and experimental studies of electromagnetic wave propagation in photonic integrated circuits with particular emphasis on devices based on silica-titania waveguide films. He is a Member of OSA.